Estimating Simulation Models of Some Hydrographic Parameters along Lake Nasser, Egypt; Applying Integration between Remote Sensing and GIS Techniques

Hussein M. El-Kobtan[*1], Islam H. Abou El-Magd[2], Mohamed Salem[3], Karima M. Attia[4], Sayed M. Ahmed[5]

[1]Nile Research Institute, National Water Research Center, Cairo, Egypt

[2]National Authority for Remote Sensing and Space Sciences, Cairo, Egypt

[3,5]Department of Geology, Faculty of Science, Benha University, Egypt

[4]Water Resources Research Institute, National Water Research Center, Cairo, Egypt

[*1]h.elkobtan@gmail.com; [2]islam.magd@gmail.com; [3]mohamedsalem199373@gmail.com; [4]karima_attia@yahoo.com; [5]smahfoz@gmail.com

Received: 24 January 2016. Revised: 7 March 2016. Accepted: 17 March 2016

Abstract- **Lake Nasser is one of the largest global man-made reservoirs, which is located on the Nile River between Latitudes of 20º27º and 23º58ºN and Longitudes of 30º07º and 33º15ºE. It stores the Egyptian and Sudanese water share budget from the Nile River catchment. The hydrographic parameters were examined to be obtained from remotely sensed satellite images, based on statistical correlation models between in-situ measurements and irradiance. These parameters include temperature, pH, total dissolved salts concentrations, electrical conductivity, turbidity and suspended sediments concentration. The statistical model was a binomial correlation between the irradiance and the in-situ measurements at the same location. Other in-situ measurements were used for the validation process, which confirmed that most of these parameters were obtained at a level of accuracy up to 80%. It has been proven that a value added decision making tool provides the operational information on the state of the lake with minimum or no field observation and low cost. The hydrographic parameters were used to provide more understanding of the ecological process rather than sedimentological one.**

Keywords- Lake Nasser; Remote Sensing; GIS, Hydrographic Parameters; Ecology; Sedimentology

I. INTRODUCTION

Egypt has constructed a large human controlled engineering structure of "High Aswan Dam" with main aim to manage the Egypt budget of Nile water resources and rescue the Nile Delta and flood plain from flooding. At the upstream side of this dam a huge reservoir was formed, which is called Lake Nasser and stores the Egyptian water budget of 55.5 BCM per year. A large amount of water flows from the catchments of the Nile River. The tunnels of the High Aswan Dam is allowed to drain downstream water to the Nile River along Lake Nasser, and the hydrographic parameters are of great importance in controlling the water quality, losses through evaporation, as well as the sedimentation processes [1].

Entz [2] studied the limnology of Lake Nasser in comparison with Lake Volta resulting in classifying Lake Nasser as an Eutrophic Lake. At early stages, the oxygen concentration of Lake Nasser was as high as 110-160% of the saturation level near the surface, caused by an intensive photosynthetic rate which is responsible for the elevated pH levels [2]. However, salt balance simulation model for Lake Nasser produced by Guariso et al. [3] found that water salinity is high during the high flood years due to the higher rates of evaporation. The seasonal and regional variations of major cations (including Na^+, Ca^{2+}, Mg^{2+}, and K^+) and major anions (including CO_3^{2-}, HCO_3^-, Cl^- and SO_4^{2-}) in Lake Nasser were studied by Saad and Goma [4, 5]. They concluded that the factors responsible for the distribution of cations and anions are the movement of water masses, adsorption on and desorption from suspended matter, transportation of eroded materials into the lake and the evaporation processes. However, Toufeek and Korium [6, 7] deduced that the concentration of major cations and anions in the flood water, along the southern part of the lake, are seasonally variable according to the change in physico-chemical parameters. On the other hand, the concentration of 38 trace elements in the lake water, after and before the flood, was determined by Sherief et al. [8].

Some of the physical and chemical hydrographic characteristics of Lake Nasser during the period from March 1982 to February 1984 were investigated through studying the Nile Phytoplankton in Egypt by Ahmad et al. [9]. They concluded that the seasonal thermal variations leads to a thermal stratification of the lake water during the period between the late spring and early autumn, whereas oxygen content appeared to vary with the changes of pH value.

It is well recognized that the essential controlling parameters in this environment are temperature, turbidity, total suspended solids concentration (TSS), total dissolved salts concentration (TDS), electrical conductivity (EC) and water power of the hydrogen ion (pH). Traditional in-situ measurements of point locations are normally used to periodically measure these

DOI: 10.18005/JRST0401006

variables and evaluate the status of the water. To understand the limnology of Lake Nasser and obtain an informed decision making regular information on the environmental status of the Lake, remotely sensed data could be used as an operation tool to provide such information. Remote sensing has been proved to be an efficient tool for provide synoptic views of physical conditions (such as currents, temperature, humidity), water quality parameters (such as phytoplankton, turbidity), and watershed characteristics (such as land classification, mangrove detection) [10-17]. Abou El-Magd and Ali, E. M. [18] developed a model to estimate the chlorophyll concentration and distribution in the largest coastal lakes of Egypt (Lake Manzala).

This research aims at functioning remotely sensed data to estimate the hydrographic physico-chemical and geomorphological parameters along the lake. These parameters include the hydro-ecological factors that affect the distribution and characteristics of the lake sediments. Then, geospatial analyses were carried out to map and model the spatial data sets of the hydrographic parameters. This might provide valuable scientific explanations for the sedimentological and geological processes of Lake Nasser.

A. Description of the Study Area

Lake Nasser (Fig. 1) lies between Latitudes of 20° 27′ and 23° 58′ N and Longitudes of 30° 07′ and 33° 15′ E. In the case of full storage capacity, the water level reaches +182 m (ASL), and the lake extends from the High Aswan Dam (HAD) in Egypt to Dal Cataract in Sudan with a length of about 500 km (about 350 km in Egyptian territory and 150 km in Sudan). In this case, the lake occupies an area of about 6500 km^2, whereas its storage capacity reaches about 162 billion m^3. This creates a maximum width of about 24 km and a maximum depth of about 110 m. The areas surrounding the lake are characterized by sandy and rocky deserts of high relief. Lake Nasser is located in the Nubian Desert, which can be climatically classified as a hyper-arid, hot, very dry desert [19]. The air temperature reaches as high as 45^{o}C in June and as low as 5^{o}C in January.

The major irregularities of the lake shape can be spatially differentiated around the plane of disconformity at Gomay into two main parts [20]. The southern geographic part located between Dal Cataract and Gomay of about 120 km length, along which the course of the lake is relatively narrow where it passes through Neoproterozoic basement rocks. The northern geographic part located between Gomay and the High Dam of about 370 km length. Along this part, the course of the lake is relatively wide where it passes mainly across a succession of sedimentary rocks from Paleozoic to Mesozoic (Upper Cretaceous).

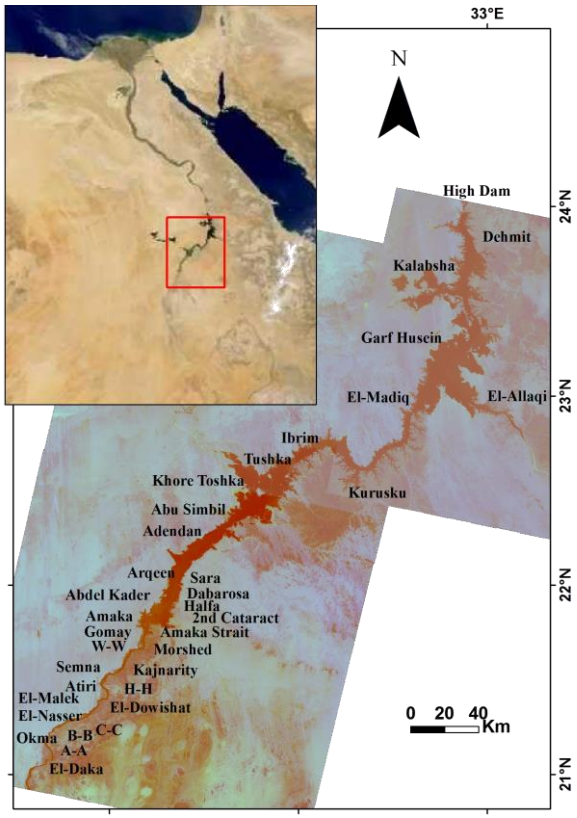

Fig. 1 Location Map of Lake Nasser

DOI: 10.18005/JRST0401006

II. MATERIAL AND METHODS

Some measuring and sampling processes were carried out through a field trip of two phases between latitudes 21° 02' 33" N and 23° 38' 55" N and longitudes 30° 38' 42" E and 32° 54' 23" E. The first phase was between 1 and 18 December 2006 covering the Egyptian part of the lake, whereas, the second phase was between 2 and 14 February 2007 covering the Sudanese part. Through this field trip, the measurements of some hydrographic physico-chemical parameters included EC, pH, and water temperature. However, the sampling processes were carried out for the lake water to be analyzed in the laboratory for determining TSS and TDS concentrations. Fig. 2 shows the vertical distribution of the investigated hydrographic parameters along the lake.

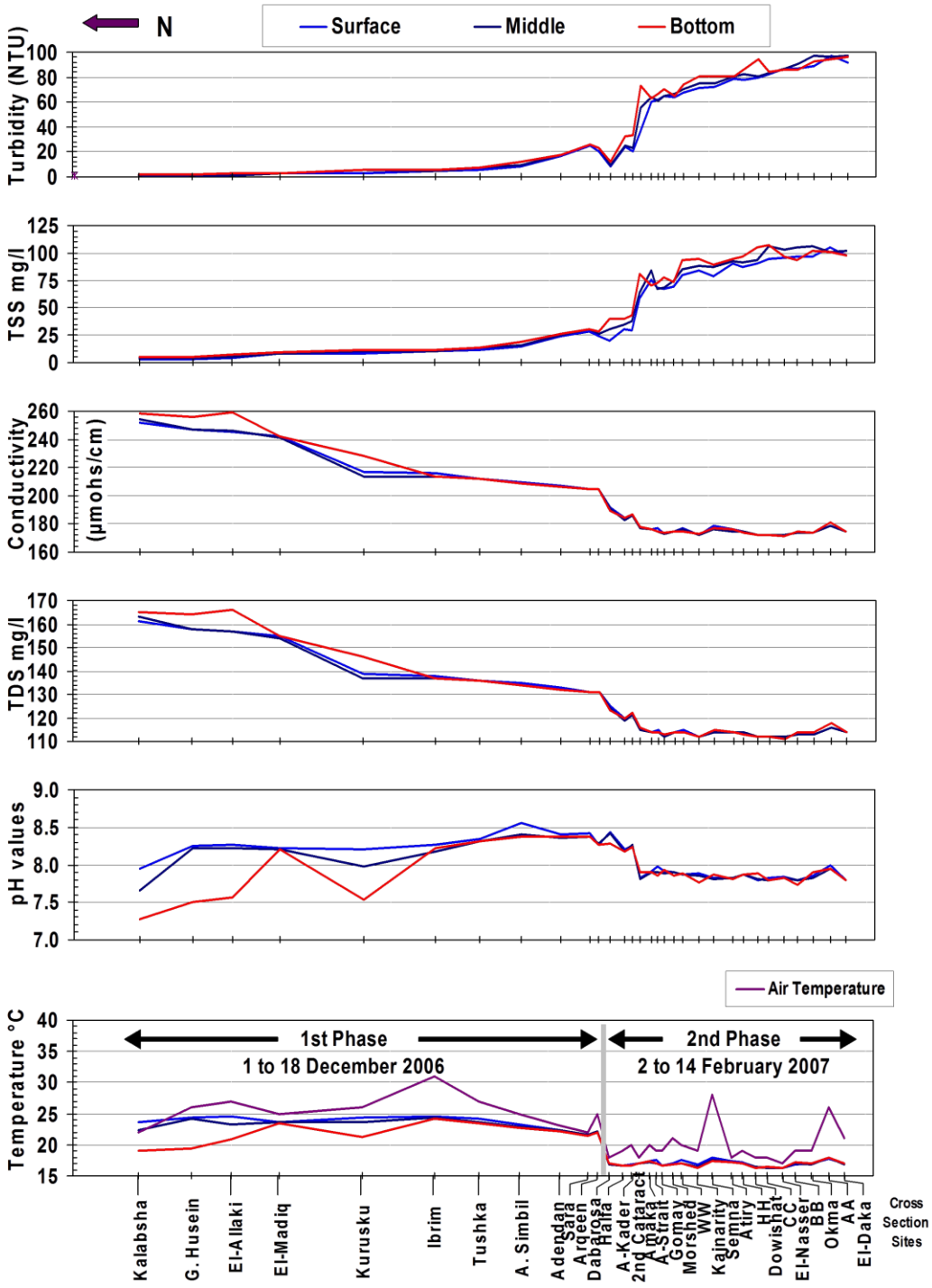

Fig. 2 Vertical distribution of the investigated hydrographic parameters along the lake

DOI: 10.18005/JRST0401006

Landsat 7 Satellite Images of level one product were selected to cover the area of Lake Nasser during the periods of the first field trip. The ERDAS Imagine 9.2 and ENVI 4.7 software programs were used for the optical and mathematical treatments and spectral analyses of the satellite images.

The integration between Remote Sensing (RS) techniques and Geographical Information Systems (GIS) provides a powerful tool to analyze and interpret the geological data. ArcGIS 9.3 software program was used for representing the spatial distribution of the hydrographic parameters. The raster patterns representing the distribution of the estimated values of the investigated hydrographic parameters were produced using this software program. The cartographic utilities of the ArcGIS software program were used for producing representative maps showing the various features and locations.

ERDAS Imagine software was used to fill the gaps and correct the errors caused by the 2003 scan line corrector failure. Using ENVI software program, the pixel values (DN) of the treated images were mathematically converted to radiance and corrected to overcome the errors belonging to the top-of-atmosphere (TOA) temperatures.

These gaps filled atmospherically with corrected radiance images were used to build a composite mosaic (Fig. 3). This mosaic simultaneously represents the lake and its landscape during the field trip with its two phases.

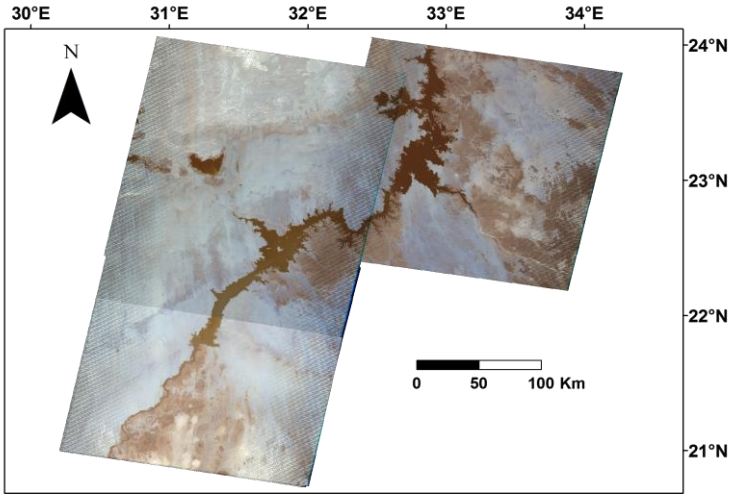

Fig. 3 A Landsat mosaic represents the lake and the surrounding landscape during the field trip (with its two phases).

Using ArcGIS software program, the pixel values at the locations of the field measuring stations, for the bands number (1 to 5), were identified. Interrelations between the pixel values of each band and the variances representing each of the field measured hydrographic parameters along the lake were investigated. Using the Microsoft Office Excel 2003 program, the linear correlation coefficients (R) were examined. The best regression equations were built to fit the most representative interrelations through attaining the highest coefficients of determination (R^2).

Using ENVI software program, the stacked banded image representing the lake water exposure was mathematically processed. This process was carried out through applying the selected best regression equation for each of the hydrographic parameters. The resultant is a raster pattern forming a two dimensional diagram representing the spatial distribution of the investigated hydrographic parameter. This representative raster pattern was processed using the ArcGIS cartographic utilities for creating appropriate layout view representing the distribution model of this parameter.

III. RESULTS AND DISCUSSION

The multi-banded image was mathematically processed using ENVI software program, through applying the best regression equation. The distribution model of each of the hydrographic parameters along the lake was produced. The ArcGIS cartographic utilities were used for creating the simulation model representing the spatial distribution of each of the hydrographic parameters.

A. Spatial variation of turbidity

The highest linear correlation coefficient (R = 0.97) characterized the interrelation between the field measurements of the average turbidity (in NTU) and the quotient of band 4/ band 1, b4/b1 (Fig. 4). The best regression equation fitting the interrelation ($R^2 = 0.94$) can be mentioned as follow;

$$y = -228.04x^2 + 377.99x - 32.63 \quad (1)$$

where y is the estimated turbidity value and x is the quotient value of b4/b1.

DOI: 10.18005/JRST0401006

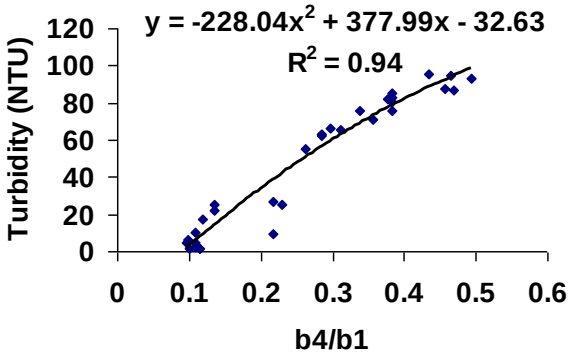

Fig. 4 Polynomial correlation between the average field measurements of turbidity and the irradiance of (b4/b1) along the lake

Using ENVI software program, the multi-banded image was mathematically processed through applying this regression equation to produce the distribution model of turbidity along the lake. The ArcGIS was used for creating the simulation model representing the spatial distribution of turbidity (Fig. 5).

The highest turbidity values were estimated along the relatively narrow and shallow southern geographic part to reflect the correlation between the high TSS, rapid flow currents, low TDS, low EC, low pH. However, the estimated turbidity values decreased northward along the relatively wide, deep lake course of the northern geographic part. The turbidity values estimated from the satellite images showed the minimum along the part of the lake north of Abu-Simbil to reflect the correlation between the low TSS, slow flow currents, relatively high pH, TDS and EC.

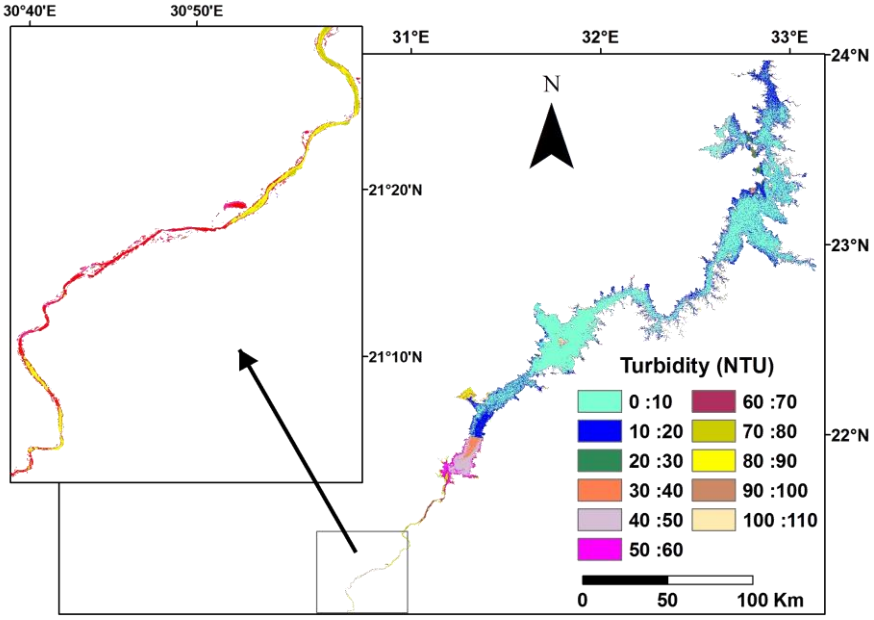

Fig. 5 Simulation model of the spatial distribution of the turbidity values estimated from satellite images along the lake

B. Spatial Variation of TSS

The highest linear correlation coefficient (R = 0.97) characterized the interrelation between the average values of the in-situ TSS measurements and the quotient of b4/b1 (Fig. 6). The best regression equation fitting the interrelation (R^2 = 0.96) can be mentioned as follow;

$$y = -302.88x^2 + 440.4x - 33.28 \quad (2)$$

where y is the estimated TSS concentration value and x is the quotient value of b4/b1.

DOI: 10.18005/JRST0401006

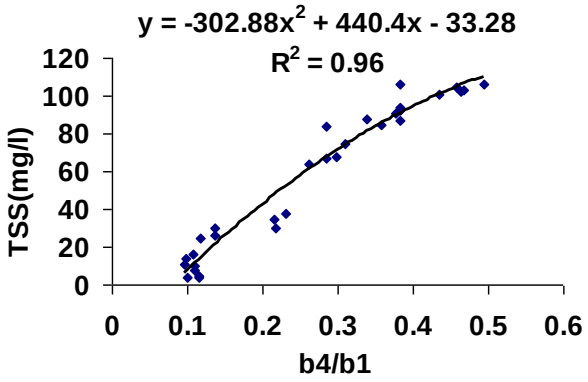

Fig. 6 Polynomial correlation between the in-situ measurements of TSS concentration and the irradiance of (b4/b1) along the lake

Applying this regression equation, the simulation model representing the spatial distribution of the average TSS values along the lake was produced (Fig. 7). This simulation model of TSS shows that the highest value estimated in the south reflects the correlation between high turbidity and high current velocity. However, the estimated values of TSS showed a northward decrease reflecting the increase of the profile area and the decrease of the current velocity.

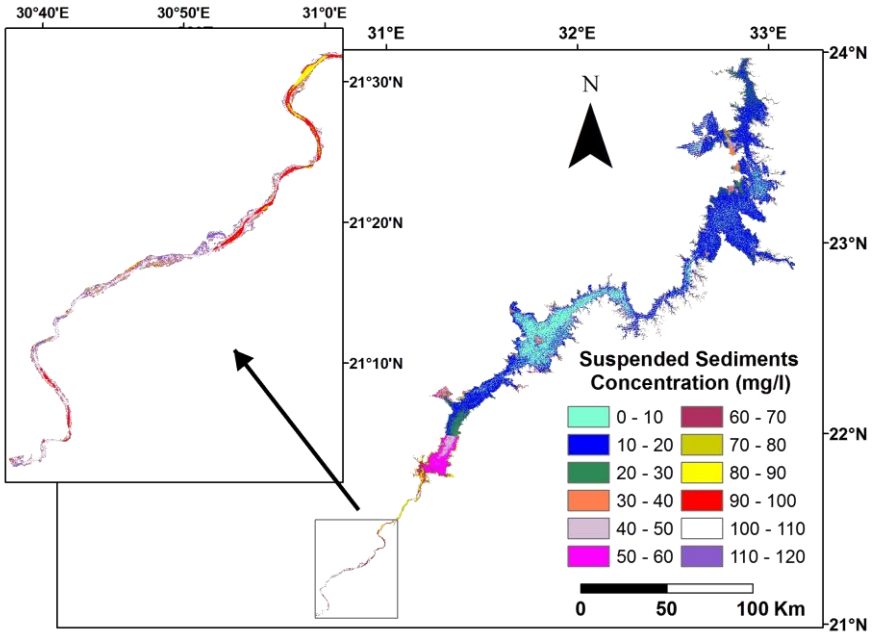

Fig. 7 Simulation model of the spatial distribution of the TSS concentration along the lake estimated from satellite images

C. Spatial Variation of EC

The highest linear correlation coefficient (R = -0.90) characterized the interrelation between the average values of the in-situ measured EC and the quotient of b3/b1 (Fig. 8). The best regression equation fitting the interrelation (R^2 = 0.84) can be mentioned as follow;

$$y = 213.59x^2 - 367.11x + 333.76 \quad (3)$$

where y is the estimated EC values and x is the quotient value of b3/b1.

Applying this regression equation, the simulation model representing the spatial distribution of the EC average values along the lake was produced (Fig. 9).

The lowest EC values estimated from satellite images along the southern geographic part reflect the relatively low TDS, low pH and high TSS. Along the northern geographic part, as the profiles became largely wider and deeper, the estimated EC values gradually increased to reach the maximum north of El-Madiq. The estimated EC values along this part of the lake reflect the correlation between the slow currents, low TSS and high pH.

DOI: 10.18005/JRST0401006

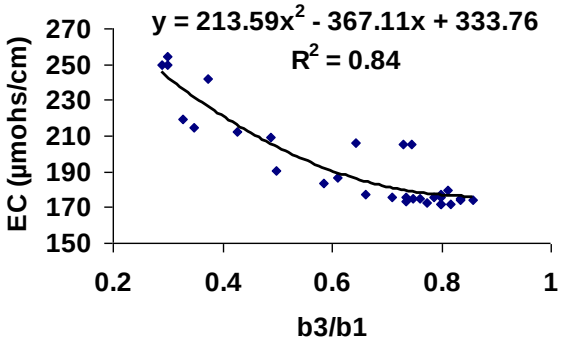

Fig. 8 Polynomial correlation between the field measurements of EC and the irradiance of (b3/b1) along the lake

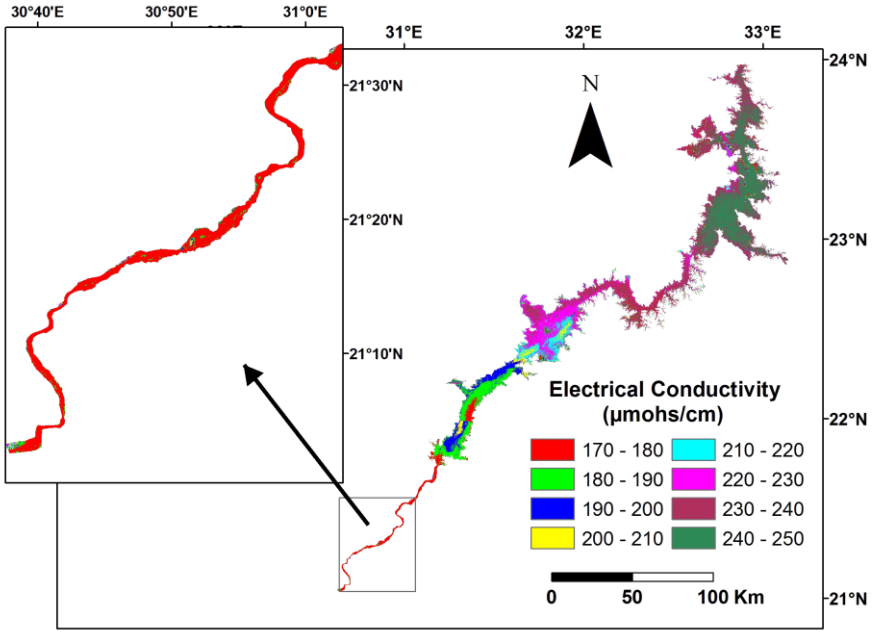

Fig. 9 Simulation model of the spatial distribution of the EC along the lake estimated from satellite images

D. Spatial Variation of TDS Concentration

The highest linear correlation coefficient (R = -0.90) characterized the interrelation between the average values of the in-situ measured TSS and the quotient of b3/b1 (Fig. 10). The best regression equation fitting the interrelation (R^2 = 0.85) can be mentioned as follow;

$$y = 132.33x^2 - 226.83x + 211.52 \quad (4)$$

where y is the estimated TDS concentration value in mg/l and x is the quotient value of b3/b1.

Applying this regression equation, the simulation model representing the spatial distribution of the TDS along the lake was produced (Fig. 11). The lowest TDS concentrations were estimated from satellite images along the narrow profiled southern geographic part. Along the northern geographic part, as the hydrographic parameters increased northward, the estimated TDS concentrations gradually increased. This increase reflects the correlation with the current velocity, TSS and pH to reach its maximum north of El-Madiq. The distribution of the estimated TDS concentrations is largely resembles that is shown by the EC.

DOI: 10.18005/JRST0401006

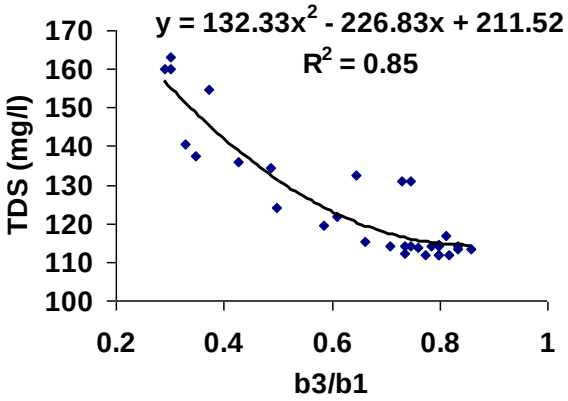

Fig. 10 Polynomial correlation between the field measurements of TDS concentration and the irradiance of (b3/b1) along the lake

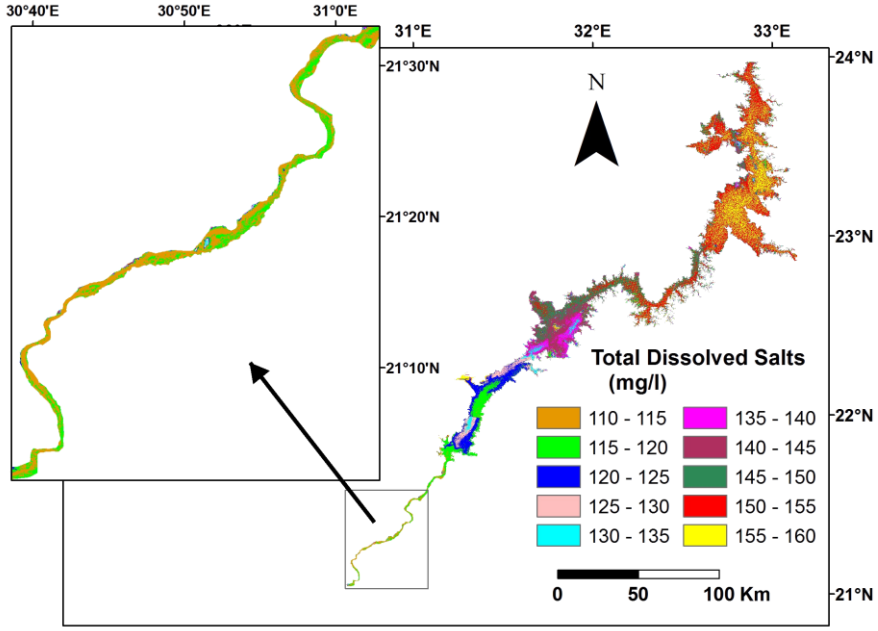

Fig. 11 Simulation model of the spatial distribution of the TDS concentration along the lake estimated from satellite images

E. Spatial Variation of pH Values

The statistical correlation between the in-situ measurements of pH of the surface layer and the irradiance of b4/b2 (Fig. 12) showed a high reverse correlation (R = -0.84). The best regression equation fitting the interrelation (R^2 = 0.75) was mentioned as follow;

$$y = 4.0464x2 - 4.0187x + 8.8257 \quad (5)$$

where y is the estimated pH values and x is the value of b4/b2.

Applying this regression equation on the multi-banded mosaic, simulation model representing the spatial distribution of the surface pH values along the lake was produced (Fig. 13). The lowest pH values (slightly alkaline) were estimated along the southern geographic part. These estimates reflect the correlation of the relatively narrow lake course, rapid flow currents, high TSS and low TDS values. Along the northern geographic part, the estimated pH values gradually increased to reach its maximum by Abu-Simbil. These estimates reflect the correlation between the slowing current velocity, lowering TSS and increasing TDS. Further northward, the estimated pH values gradually decreased to reflect the increasing current velocity and bottom depth towards the High Aswan Dam.

DOI: 10.18005/JRST0401006

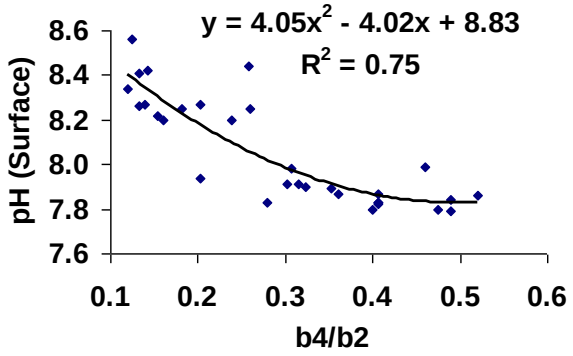

Fig. 12 Polynomial correlation between the field measurements of the surface pH values and the irradiance of (b4/b2) along the lake

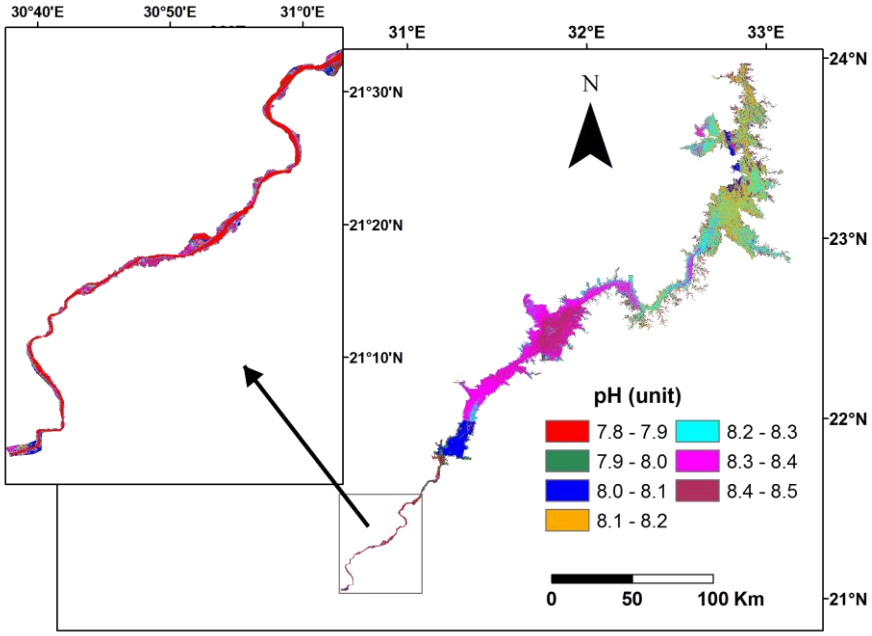

Fig. 13 Simulation model of the spatial distribution of the surface pH values estimated from satellite images along the lake

F. Spatial Variation of Water Surface Temperature

Temperature is a very fundamental factor in the hydrological changes, sediment transportation and sediment-water interaction. Water has a high thermal inertia, that it changes temperature slowly as heat energy is added, a low thermal conductivity, that heat passes through it slowly, and a high thermal capacity, that it stores heat well [21]. Therefore, huge water bodies like Lake Nasser can keep heat for periods of time sufficient to be sensed remotely.

To estimate the surface temperature from remotely sensed data and its distribution along the lake during the two periods of the field trip, the previously explained Landsat 7 images were used. These images were captured in the thermal infrared that could be converted into surface temperature using the following equation;

$$T = K_2 / \ln\left(\frac{K_1 * \varepsilon}{L_\lambda} + 1\right) \quad (6)$$

where,

T= Brightness temperature in Kelvin;

L_λ= is the atmospherically corrected cell value as radiance (Watts/ (m^2 * srad * μm));

K_1 and K_2 = Band-specific thermal conversion constant given by the Landsat 7 Science Data Users Handbook [22] from NASA for the bands number B6_VCID_1 and B6_VCID_2

= 666.09 & 1282.71 for the Landsat 7 ETM+;

E= is the emissivity factor.

DOI: 10.18005/JRST0401006

NASA 1999 published global maps for surface emissivity to be used in satellite retrievals of long-wave radiation. The landscape of the study area composed of the lake water surface and the rock exposures which were covered with sand sheets in some parts. Depending on the algorithms provided by the above mentioned satellite spectral data sources, the mean value of emissivity for water and rocky sandy landscape in the arid North African regions were estimated as about 0.986 and 0.95 respectively. The produced three thermal images representing the radiance values of band 6 in Kelvin degrees were used to build a mosaic for the lake and its surrounding area during the two phases of the field trip (Fig. 14).

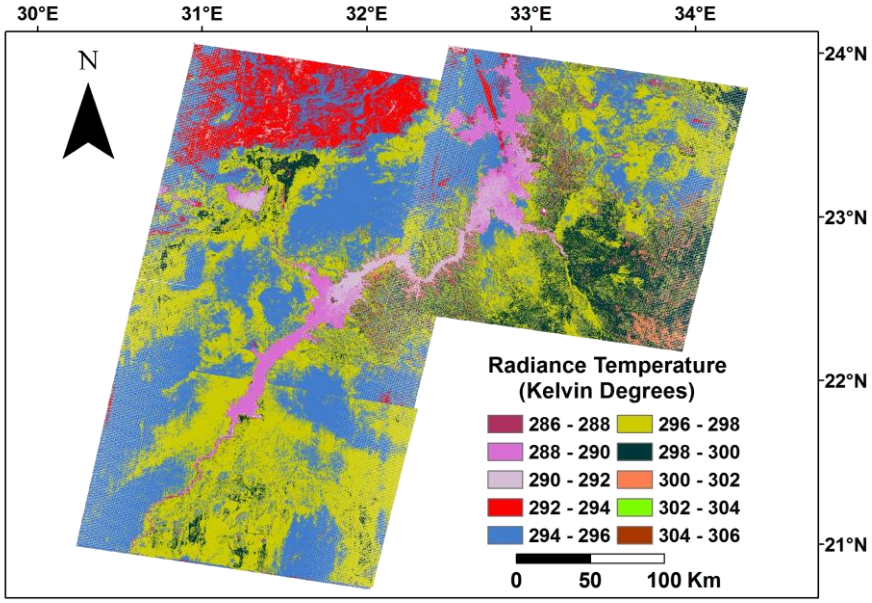

Fig. 14 The distribution of the radiance thermal temperature values in Kelvin degrees for the lake and the surrounding areas during the two phases of the field trip

ArcGIS 9.3 software was used to crop a mosaic to estimate the spatial surface thermal distribution in Kelvin along the lake water mass (Fig. 15).

The interrelation between the in-situ measured surface water temperature and the corresponding radiance temperature (pixel values) was investigated. Along the 90 km distance between El-Daka and Semna (mainly, the riverine environment), this interrelation showed no obvious correlation. This may be due to the difference in time of measurements and capturing the images and to the relatively rapid flow and the shallowness of the lake course, as well. Whereas, along the rest 410 km of the lake length (mainly, the lacustrine environment), the interrelation (Fig. 16) showed a linear relationship with a correlation coefficient ($R = 0.89$).

DOI: 10.18005/JRST0401006

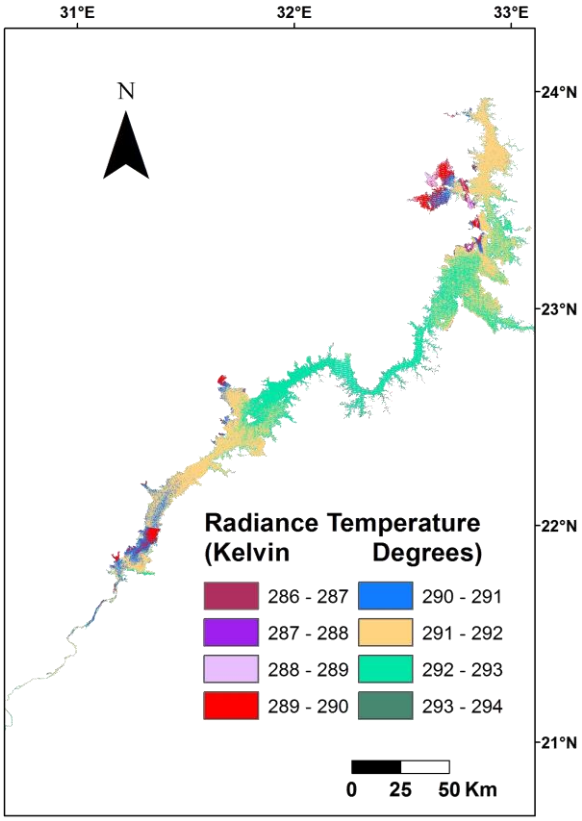

Fig. 15 Simulation model of the estimated spatial thermal surface distribution in Kelvin along Lake Nasser water mass during the two phases of the field trip

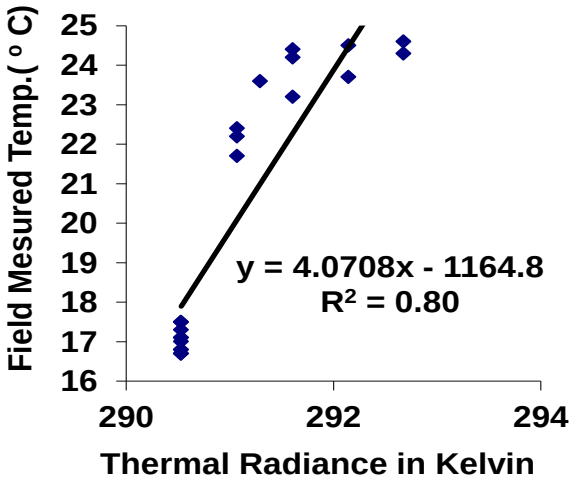

Fig. 16 An interrelation between the radiance temperature and the in-situ measured surface water temperature in the north of Semna

The best regression equation fitting the interrelation ($R^2 = 0.800$) can be mentioned as follow;

$$y = 4.0708x - 52.853 \quad (7)$$

where,

y = actual surface water temperature measured during the field trip in Celsius degrees;

x = pixel values for radiance temperature in Kelvin.

The pixel thermal values in Kelvin degrees, of the part of the lake water mass downstream Semna, were converted to Celsius degrees, using ENVI software program, by applying the mathematical formula:

DOI: 10.18005/JRST0401006

$$°C = K - 273.15 \quad (8)$$

where °C is the temperature in Celsius degrees and K is the temperature in Kelvin.

Fig. 17 is a simulation model shows the thermal spatial distribution in Celsius degrees along this part of the lake. The remotely sensed thermal distribution is considerably matching with the actual in-situ measurements.

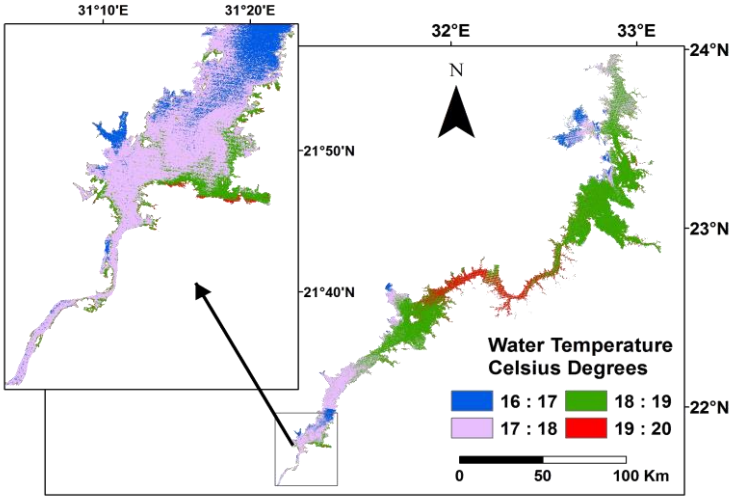

Fig. 17 Simulation model of the estimated spatial surface temperature distribution in Celsius degrees along the part of the lake downstream Semna

IV. CONCLUSIONS

Remotely sensed data has shown an efficient tool to estimate the hydrographic parameters in Lake Nasser, however GIS was an effective geospatial analysis platform. All of these parameters are highly correlated to the irradiance of the affected bands through binomial interrelations. The spatial distribution of each parameter was estimated on a pixel base along the lake water mass.

The patterns of distribution along the southern part showed that TDS ranged from 110 to 120 mg/l, EC from 170 to 180, surface pH from 7.8 to 7.9, turbidity from 50 to 100 NTU and TSS ranged from 70 to 120 mg/l. These estimates largely resemble the ranges of the in-situ measurements. Along the northern part (south of Abu-Simbil), as the total dissolved salts increased to reach values between 115 and 135, EC between 170 and 210, surface pH between 8 and 8.4, TSS decreased to reach values between 10 and 50 mg/l and, accordingly, turbidity decreased to reach values between zero and 30 NTU. However, in the north of Abu-Simbil, as the TDS increased to range from 130 to 160 mg/l, EC increased northward from 210 to 250, surface pH decreased northward from 8.4 to 8.1, turbidity decreased to values less than 20 NTU and the TSS decreased to range from 0 to 20 mg/l.

It may be recommended for future work for a further improve of the geospatial database for creating a GIS model to facilitate a routinely estimation of each of the hydrographic parameters on regular bases. This could be carried out through the regular correlation of the field measurements with the irradiance of the satellite images.

REFERENCES

[1] H. M. El-Kobtan, "Geological studies on the recent sediments of Lake Nasser (southern part) as a sign reflecting its evolution," M. Sc. thesis, Faculty of Science, Benha University, Egypt, p. 106, 2007.

[2] B. A. G. Entz, "Comparison of the physical and chemical environments of Volta Lake and Lake Nasser," Ibp-Unesco Symposium on Productivity Problems of Freshwaters, pp. 883-891, 1972.

[3] G. Guariso, D. Whittington, A. S. Elewa and G. Kramer, "A salt balance simulation of Lake Nasser," *Water supply and Management*, pp. 73-80, 1980.

[4] A. H. Saad and R. H. Goma, "Distribution of the major ions in Lake Nasser. I- major anions," *Acta Adriatica*, vol. 33(1-2), pp. 39-48, 1992.

[5] A. H. Saad and R. H. Goma, "Distribution of the major ions in Lake Nasser. II- major cations," *Acta Adriatica*, vol. 33(1-2), pp. 25-38, 1992.

[6] M. A. Toufeek and M. A. Korium, "Factors controlling the distribution of the major metals in Lake Nasser water," *American- Urasian Agriculture and Environmental Science*, vol. 5(6), pp. 804-812, 2009.

[7] M. A. Toufeek and M. A. Korium, "Physicochemical characteristics of water quality in Lake Nasser water," *Global Journal of Environmental Research*, vol. 3(3), pp. 141-148, 2009.

[8] M. K. Sherief, R. M. Awadallah and F. Grass, "Trace elements in water samples from Lake Nasser - Lake Nubia," *Radioanalytical Chemistry*, vol. 60(1), pp. 267-272, 1980.

DOI: 10.18005/JRST0401006

[9] A. M. Ahmad, A. A. Mohamed, I. Springuel and A. M. El-Otify, "Field and laboratory studies on Nile phytoplankton in Egypt. III. Some physical and chemical characteristics of Aswan High Dam Lake (Lake Nasser)," *Internationale Revue der gesamten Hydrobiologie und Hydrographie*, vol. 74, pp. 329-348, 1989.

[10] P. Lavery, C. Pattiaratchi, A. Wyllie and P. Hick, "Water quality monitoring in estuarine waters using the Landsat Thematic Mapper," *Remote Sensing of Environment*, vol. 46, pp. 268-290, 1993.

[11] J. Liedtke, A. Roberts and J. Luternauer, "Practical remote sensing of suspended sediment concentration," *Photogrammetric Engineering and Remote Sensing*, vol. 6l(2), pp. 167-175, 1995.

[12] V. K. Chouby, "Laboratory experiment, field and remotely sensed data analysis for the assessment of suspended solids concentration and secchi depth of the reservoir surface water," *International Journal of Remote Sensing*, vol. 19(17), pp. 3349-3360, 1998.

[13] D. L. Woodruff, R. P. Stumpf, J. A. Scope and H. W. Paerl, "Remote estimation of water clarity in optically complex estuarine waters," *Remote Sensing of Environment*, vol. 68, pp. 41-52, 1999.

[14] D. Doxaran, J. M. Froidefond, S. Lavender and P. Castaing, "Spectral signature of highly turbid waters application with SPOT data to quantify suspended particulate matter concentrations," *Remote Sensing of Environment*, vol. 81, pp. 149-161, 2002.

[15] S. M. Kloiber, P. L. Brezonik, L. G. Olmanson and M. E. Bauer, "A procedure for regional lake water clarity assessment using Landsat multispectral data," *Remote Sensing of Environment*, vol. 82(1), pp. 38-47, 2002.

[16] M. Kishino, A. Tanaka and J. Ishizaka, "Retrieval of chlorophyll a, suspended solids, and colored dissolved organic matter in Tokyo Bay using ASTER data", *Remote Sensing of Environment*, vol. 99, pp. 66-74, 2005.

[17] T. G. Prescott, "Estimating temporal and spatial variations in water clarity at Lake Tahoe, California-Nevada, using ASTER multi-Spectral remote sensing data," M. Sc. thesis, University of Nevada, USA, p. 109, 2006.

[18] I. H. Abou El-Magd and E. M. Ali, "Estimating and mapping chlorophyll a concentration as a function of environmental changes of Manzala Lagoon, Egypt using Landsat 7 ETM+ Images," *Australian Journal of Basic and Applied Sciences*, vol. 2(4), pp. 1307-1314, 2008.

[19] I. V. Springuel, L. M. Hassan, M. Sheded, M. El-Soghir and M. M. Ali, "Plant ecology of Wadi Allaqi and Lake Nasser; flora of the Wadi Allaqi basin," University of Glasgow, Working Paper, No. 10, p. 14, 1991.

[20] H. El-Kobtan, M. Salem, K. Attia, S. M. Ahmed and I. Abou El-Magd, "Sedimentological study of Lake Nasser; Egypt, using integrated improved techniques of core sampling, x-ray diffraction and GIS," Conference on Role of Applied Science in Development and Community Service, Faculty of Science, Benha University, Egypt, vol. 2(4), pp. 225-241, 2015.

[21] R. N. Handcock, C. E. Torgersen, K. A. Cherkauer, A. R. Gillespie, K. Tockner, R. N. Faux and J. Tan "Thermal infrared remote sensing of water temperature in riverine landscapes," in *Fluvial Remote Sensing for Science and Management*, First Edition, Edited by Carbonneau P. E. and Herve Piegay by John Wiley & Sons, Ltd., pp. 85-113, 2012.

[22] 2011, NASA Official Website, Online, Landsat science data users handbook. Available: http://landsathandbook.gsfc.nasa.gov/pdfs/Landsat7_Handbook.pdf

DOI: 10.18005/JRST0401006